Journal of ELECTRONIC MATERIALS, Vol. 47, No. 1, 2018
DOI: 10.1007/s11664-017-5906-x

Study of Diffusion Barrier for Solder/*n*-Type Bi_2Te_3 and Bonding Strength for *p*- and *n*-Type Thermoelectric Modules

WEN-CHIH LIN,[1] YING-SIH LI,[1] and ALBERT T. WU[1,2]

1.—Department of Chemical and Materials Engineering, National Central University, Taoyuan City 32001, Taiwan. 2.—e-mail: atwu@ncu.edu.tw

This paper investigates the interfacial reaction between Sn and Sn3Ag0.5Cu (SAC305) solder on *n*-type Bi_2Te_3 thermoelectric material. An electroless Ni-P layer successfully suppressed the formation of porous SnTe intermetallic compound at the interface. The formation of the layers between Bi_2Te_3 and Ni-P indicates that Te is the dominant diffusing species. Shear tests were conducted on both Sn and SAC305 solder on *n*- and *p*-type Bi_2Te_3 with and without a Ni-P barrier layer. Without a Ni-P layer, porous SnTe would result in a more brittle fracture. A comparison of joint strength for *n*- and *p*-type thermoelectric modules is evaluated by the shear test. Adding a diffusion barrier increases the mechanical strength by 19.4% in *n*-type and 74.0% in *p*-type thermoelectric modules.

Key words: Bi_2Te_3, thermoelectric module, electroless Ni-P, diffusion barrier, interfacial reaction, shear strength

INTRODUCTION

The demands for developing renewable energy is urgent for environmental protection. Thermoelectric (TE) systems are known to convert waste heat into electrical energy, and it can be widely used in power generation and coolers. The Seebeck effect appears when providing a temperature gradient to a TE module that generates the proportional voltage between the opposing ends of the TE module. In contrast, a temperature gradient resulting from a voltage applied on a TE module is identified as the Peltier effect.[1] The efficiency of TE material is very sensitive to the applied temperature range. A bismuth telluride (Bi_2Te_3) based TE module is effective for gathering low-temperature waste heat and is commonly used in a thermoelectric generator (TEG) which operates with high efficiency below 200°C.[2] The effect of the TE module is quantified by the figure of merit, ZT, given by Eq. 1[3]:

$$ZT = \frac{s2 \cdot \sigma}{K} T, \tag{1}$$

where s is the Seebeck coefficient of the *n*- and *p*-type material, and σ, K, and T represent the conductivity, thermal conductivity and temperature, respectively. Nowadays, both $(Bi_xSb_{2-x})Te_3$ and $Bi_2(Te_{3-x}Se_x)$ are known to be the best bulk *p*-type and *n*-type TE material with a figure of merit to approximately 1 at room temperature.[2] In the module, it is important to connect these materials to electrodes, usually Cu, to conduct the converted electricity. Sn-based solder is usually selected as jointed materials between TE material and the electrodes. However, the formation of the intermetallic compound (IMC) between the TE material and solder is unfavorable due to its weak mechanical strength and high contact resistance.[4] It has been known that the formation of porous-type SnTe IMC would drastically degrade the reliability of the TEG module.[4,5] An insertion of a diffusion barrier is required to suppress the formation of the weak SnTe IMC.

Several studies have shown that Ni is an effective diffusion barrier for the module to suppress the SnTe IMC.[6–14] Electroless Ni-P is a well-developed plating method in electronic packaging. Chien et al. and Lin et al. reported electroless Ni-P layer for a diffusion barrier between solders and *p*-type

(Received July 24, 2017; accepted October 25, 2017; published online November 13, 2017)

Bi_2T_3.[9,11] However, the interfacial reaction between solders on *n*-type Bi_2Te_3 with a Ni-P layer has not been reported nor evaluated. The adhesion between a Ni-P layer on *n*-type Bi_2Te_3 was poor; the Ni layer is easily peeled off during reflow. In this study, the Ni-P layer was successfully deposited on *n*-type Bi_2Te_3 by overcoming the uneven temperature distribution during the reflow process. The interfacial reaction layers were investigated for two different solders, pure Sn and Sn3Ag0.5Cu (SAC305) that were reflowed on *n*-type Bi_2Te_3 with and without an electroless Ni-P layer.

Although SnTe can be suppressed by a Ni diffusion layer, Ni and Te also form NiTe, $NiTe_2$ or Ni_3Te_2 IMCs. The assessment of the joint strength for both *n*- and *p*-type modules have not been reported and compared. A ball shear test was applied to investigate the mechanical properties of n- and *p*-type Bi_2Te_3 without and with a Ni-P layer. Adding a diffusion barrier increases the mechanical strength by 19.4% in *n*-type and 74.0% in *p*-type thermoelectric modules. The results also show that the fracture mode for both Sn and SAC305 solder on *n*- and *p*-type Bi_2Te_3 with a Ni-P layer are ductile due to lack of porous SnTe IMC. This study confirms that a Ni-P layer can efficiently suppress the formation of porous SnTe IMC and greatly enhance the mechanical strength of the TE module.

EXPERIMENTAL PROCEDURES

Selenium (Se) was doped in Bi_2Te_3 for making *n*-type Bi_2Te_3 with the composition of $Bi_2(Te_{2.55}Se_{0.45})$. The samples were prepared by the zone melting (ZM) method and provided by Industrial Technology Research Institute (ITRI).[15] Before electroless Ni-P depositing, the surface of *n*-type Bi_2Te_3 substrate was ground and polished by 0.1-μm Al_2O_3 suspensions and then etched by HNO_3 solution for 15 min to remove impurities and increase the physical bonding between Ni-P film and substrates. An electroless Ni-P diffusion barrier layer was deposited on a *n*-type Bi_2Te_3 surface at 80 ± 5°C for 25 min. The thickness was around 10 um. Table I shows the conditions of the electroless nickel plating bath and the plating parameters.[11] Pure Sn and SAC305 solders (0.02 g) were reflowed on *n*-type Bi_2Te_3 with and without Ni-P layers. The reaction was conducted at 270°C for 30 s under five reflow cycles by using the desktop reflow oven (SANYO-SEIKO SMT Scope, SP-5000DS) at SHENMAO Technology Incorporated. After five reflow cycles, as-prepared samples were kept in the oven at 150°C for 1, 5, 10 and 15 days. Following the aging process, the samples were removed from the oven and cooled in air to room temperature. The morphology of the IMCs was observed through scanning electron microscopy (SEM, Hitachi S-3000 H). Field-emission electron probe microanalysis (FE-EPMA, JXA-8500F, JEOL) was used for analyzing the compositions of IMCs. For the ball shear test, pure Sn and SAC305 solder balls (600 μm) were reflowed on the electroless Ni-based surface finishes with an opening area of 300 μm in diameter which was defined through lithography at 270°C for 30 s under five reflow cycles. The evolution of the microstructure on mechanical properties was determined by using ball shear test equipment (Dage 4000, DAGE) to measure the shear strength with 50 μm/s impact velocity and 60 μm shear height (top of Bi_2Te_3 without Ni-P and top of Ni-P after depositing). In this study, each data point was included from an average of 15 measurements.

Table I. Conditions of electroless nickel bath and plating parameter

$NaH_2PO_2{\cdot}H_2O$	27 g/L
$NiSO_4{\cdot}6H_2O$	20 g/L
$Na_2C_4H_4O_4{\cdot}6H_2O$	16 g/L
Bath temperature	80 ± 5°C
Plating time	25 min
PH	5.8

RESULTS AND DISCUSSION

Interfacial Reaction of Solder/*n*-Type Bi_2Te_3 and Solder/Ni-P/*n*-Type Bi_2Te_3

Figure 1a presents the schematic plot of solders reflowed on *n*-type Bi_2Te_3 without and with Ni-P layers. Figure 1b and c show the backscattered electron images (BEI) of pure Sn and SAC305 solders that reacted with *n*-type Bi_2Te_3 substrate for five times reflow at 270°C for 30 s. These samples were then aged at 150°C for 1, 5, 10 and 15 days. Since the phases at the interfaces could not be clearly identified from Fig. 1, both Sn/*n*-type Bi_2Te_3 and SAC305/*n*-type Bi_2Te_3 are reflowed for 15 min at 270°C and are shown in Fig. 2. Figure 2a and b show the enlarged images for the interface regions. It can be seen that two layers of IMCs grew between the solders and the TE materials. Based on the elemental EPMA analysis, the dark region is a SnTe compound. Another thin bright compound layer could be seen between SnTe and *n*-type Bi_2Te_3. The elemental analysis identified the layer as Bi_4Te_3. Bos et al. and Lo et al. suggested an infinitely adaptive series of $(Bi_2)_m(Bi_2Te_3)_n$ would be produced during the phase transformation from Bi_2Te_3 to Bi_4Te_5 when there is a deficiency of Te.[16,17] In this study, the Te near the interface was massively consumed during the formation of SnTe, the depleted Te would result in the formation of Bi_4Te_3. After aging for 15 days, the thickness of SnTe grew with increasing aging time, and the thicknesses were around 7 μm in Sn/*n*-type Bi_2Te_3 and 7.5 μm in SAC305/*n*-type Bi_2Te_3, respectively. Figure 3 plots the thickness of SnTe IMCs as the function of aging time. Because the melting point of SAC305 is lower than Sn solder, the reaction in the SAC305/*n*-type Bi_2Te_3 is expected to be faster than

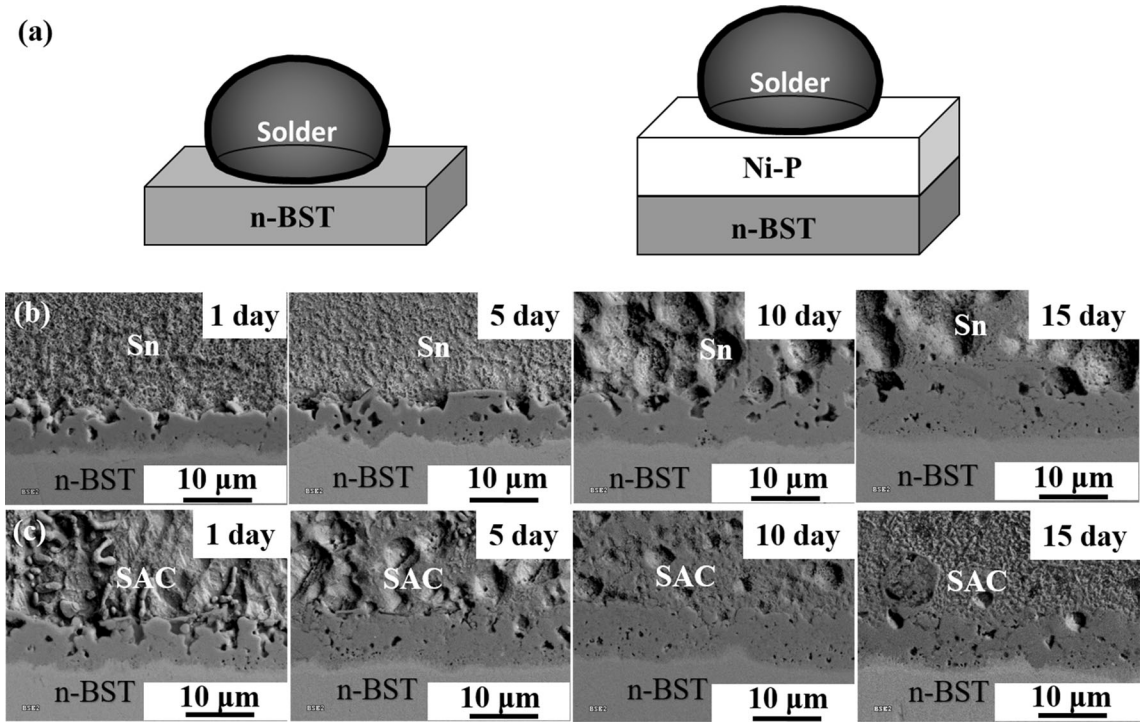

Fig. 1. (a) A schematic plot of solder reflowed on *n*-type Bi_2Te_3 without and with Ni-P layers and cross-section BEI images of (b) Sn/*n*-type Bi_2Te_3 (c) SAC305/*n*-type Bi_2Te_3 aged at 150°C for 1, 5, 10 and 15 days.

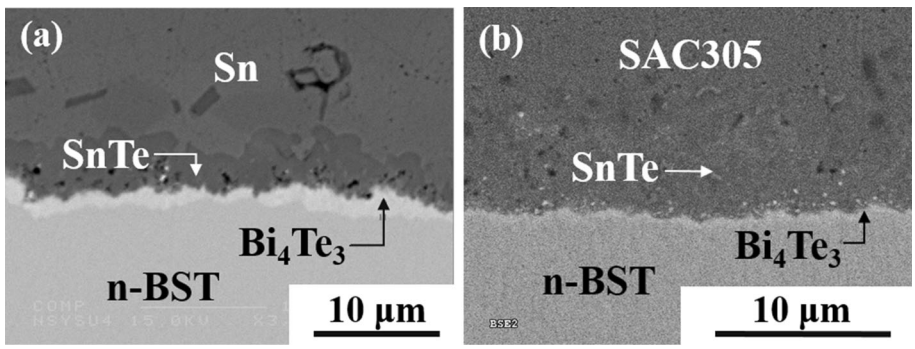

Fig. 2. Cross-section EPMA images of (a) Sn/*n*-type Bi_2Te_3 (b) SAC305/*n*-type Bi_2Te_3 reflowed for 15 min at 270°C.

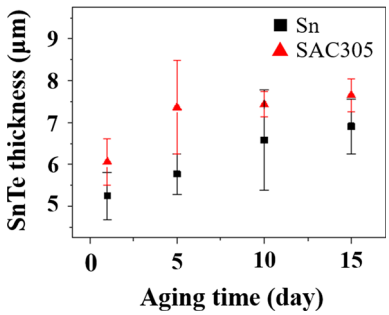

Fig. 3. The thickness of SnTe as a function of aging time for Sn and SAC305 solders.

the Sn/*n*-type Bi_2Te_3. Hence, the thickness of SnTe in SAC305/*n*-type Bi_2Te_3 is thicker than Sn/*n*-type Bi_2Te_3. Comparison of the thickness of SnTe IMC in solder/*n*-type Bi_2Te_3 with that in solder/*p*-type Bi_2Te_3 has been reported.[18,19] The Bi content in *n*-type Bi_2Te_3 for this study is 40 at.%. It is higher than the conventional Bi content, 10 at.%, in *p*-type Bi_2Te_3. Liao et al.[18] suggested that the dissolution of Bi would inhibit the growth of SnTe. Chen et al.[19] observed the thickness of SnTe IMC in Sn/*n*-type Bi_2Te_3 is smaller than that in Sn/*p*-type Bi_2Te_3, and they proposed that it might be due to the addition of a small amount of Se. Despite different reaction rates, porous SnTe grows in both *n*- and *p*-type TE systems.

After electroless Ni-P plating on *n*-type Bi_2T_3, no SnTe IMC was observed after a long time for the thermal aging process. Figure 4 shows the Sn and SAC305/Ni-P/*n*-type Bi_2Te_3 system reflowed for five

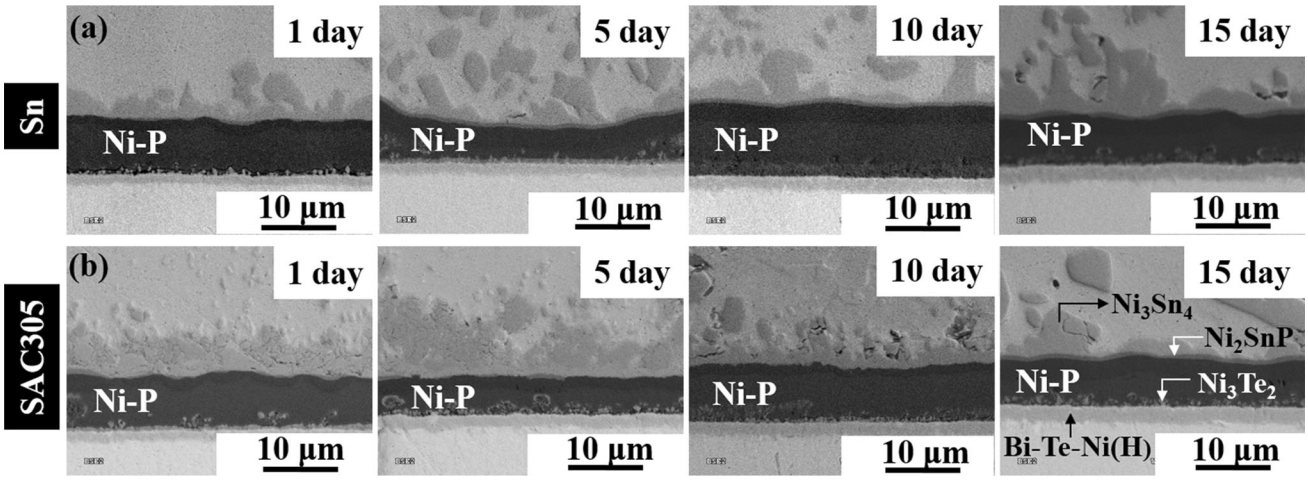

Fig. 4. Cross-section BEI images of (a) Sn/Ni-P/*n*-type Bi_2Te_3 (b) SAC305/Ni-P/*n*-type Bi_2Te_3 aged at 150°C for 1, 5, 10 and 15 days.

cycles at 270°C for 30 s and followed by aging for 1, 5, 10 and 15 days at 150°C. EPMA was introduced to characterize the composition of the IMCs. Since the layers in Fig. 4 are not thick enough to be identified, both Sn/Ni-P/*n*-type Bi_2Te_3 and SAC305/Ni-P/*n*-type Bi_2Te_3 were reflowed for 15 min at 270°C and are shown in Fig. 5. Figure 5a is the identification of the phases in the Sn/Ni-P/*n*-type Bi_2Te_3. Ni and Sn formed Ni_3Sn_4 intermetallic compound in the Sn matrix. A layer of Ni_2SnP grew between Ni_3Sn_4 and Ni-P. Figure 5b shows a modified contrast and brightness of 5 (a) to clearly reveal three IMCs layers in the electroless Ni-P layer. Figure 5b shows the top layer was Ni_2P phase, middle layer was Ni_3P and the bottom layer was electroless Ni-P. Lin et al.[20] recently proposed that the formation of Ni_2SnP was related to metastable Ni_2P in the Ni-P phase diagram. In order to decrease Gibbs free energy, Sn atoms easily diffused into Ni_2P and formed Ni_2SnP rather than diffused into Ni_3P, which is a stable state in the Ni-P phase diagram. In the SAC305/Ni-P/*n*-type Bi_2Te_3 system, the interface reaction of IMCs is similar to the Sn/Ni-P/*n*-type Bi_2Te_3 system, as shown in Fig. 5c. The only difference is that the Ni_2P phase did not form at the SAC305/Ni-P interface. At the TE side, two layers of Bi-Te-Ni could be identified. The one adjacent to the Ni-P layer has the average composition of Bi-28.71 at.% Te-45.84 at.% Ni (Bi-Te-Ni(H)). Another Bi-Te-Ni layer could be observed in the *n*-type Bi_2Te_3 side. The elemental composition was Bi-38.44 at.% Te-15.56 at.% Ni (Bi-Te-Ni(L)). This layer cannot be observed in the thermal aging samples, and it is believed to be a metastable phase. It can be seen from Fig. 4 that the size of Ni_3Sn_4 becomes bigger, and the IMC spalls into solder due to the formation a Ni-Sn-P layer with increasing aging time. The thickness of Bi-Te-Ni(H) would increase and indicate a continuous interdiffusion of Ni and Te. On the contrary, the thickness of Ni-P layer was almost constant during aging. From the results, we found that an electroless Ni-P film would effectively suppress diffusion of Sn at 270°C for 15 min and confirmed that electroless Ni-P is an effective diffusion barrier for the interfacial reaction between solders and *n*-type Bi_2Te_3.

A schematic plot of the atomic diffusion mechanism in the Ni-P/*n*-type Bi_2T_3 reaction is presented in Fig. 6. We speculated that Te atoms would rapidly diffuse into the electroless Ni-P layer and form Ni_3Te_2. Chen et al.[10] suggested that Te is the fastest diffusion species under thermal treatment in Ni/*n*- and *p*-type Bi_2Te_3. With increasing reflow time, Ni would diffuse into the *n*-type Bi_2Te_3 substrate and form the Bi-Te-Ni(H) phase, which had a high atomic concentration of Ni. Te atoms would simultaneously diffuse toward Ni-P layers while Ni keeps moving toward the *n*-type Bi_2Te_3 substrate. Thus, the Te concentration near the interface was reduced but increased Bi content since the diffusion of Bi is slow in the system.[5,10] A new Bi-Te-Ni(L) layer, which had a lower atomic concentration of Ni, would form adjacent to Bi-Te-Ni(H).

Mechanical Properties of Electroless Ni-P on Thermoelectric Modules

The interfacial reaction of solder/*p*-type Bi_2Te_3 and solder/Ni-P/*p*-type Bi_2T_3 has been reported in the literature.[11] This study focuses on the mechanical properties of solder on both *n*- ($Bi_2(Se_{0.45}Te_{2.55})$) and *p*-type Bi_2Te_3 ($(Bi_{0.25}Sb_{0.75})_2Te_3$) with and without Ni diffusion barriers. To identify whether electroless Ni-P affects the reliability of solder joints, a ball shear test was performed to evaluate mechanical strength. Figure 7a and b present the results of tests conducted using 50-μm/s impact velocity and 60-μm shear height in *n*- and *p*-type Bi_2Te_3 systems. The shear strength approximately improved 4 MPa in *n*-type Bi_2Te_3 and 10 MPa in *p*-type Bi_2Te_3 after depositing

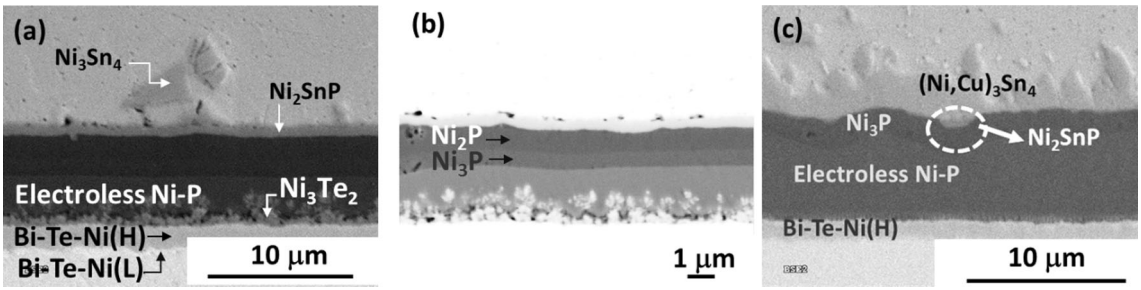

Fig. 5. Cross-sectional EPMA images of (a) Sn/Ni-P/*n*-type Bi_2Te_3 (b) Images corresponding to (a) with modified contrast (c) SAC305/Ni-P/*n*-type Bi_2Te_3.

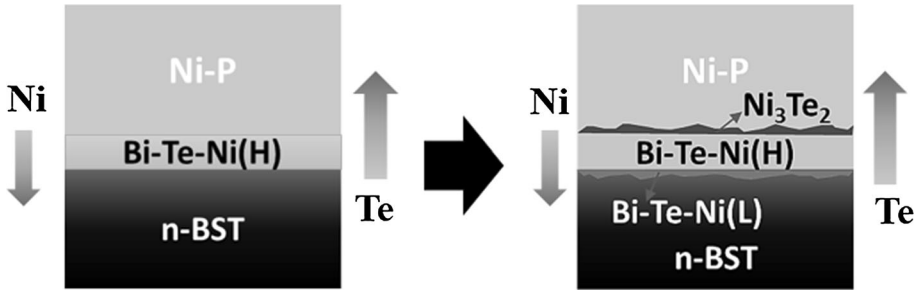

Fig. 6. A schematic plot of the atomic diffusion mechanism in Ni-P/*n*-type Bi_2Te_3 reaction.

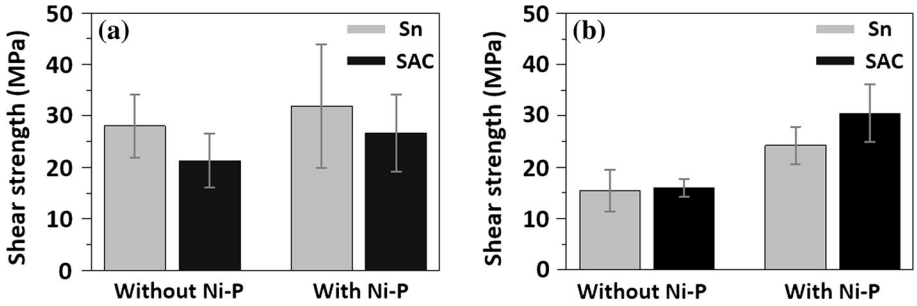

Fig. 7. The results of shear tests conducted using 50 μm/s impact velocity and 60 μm shear height for (a) *n*type Bi_2Te_3 (b) *p*-type Bi_2Te_3.

Ni-P layers in both systems. Adding a diffusion barrier increases the mechanical strength by 19.4% in *n*-type and 74.0% in *p*-type thermoelectric modules. The lower strength obtained from the system without Ni-P could be due to the formation of porous SnTe IMC.

In general, when conducting a shear test, it is desirable to rupture in the solders rather than substrate and thus prevent the damage to the substrate. In the *n*-type Bi_2Te_3 system, the top views of the fracture surfaces of the solder joints after shear tests are shown in Fig. 8a. The fracture surfaces are divided into three modes: mode A is cracking in the solder, and the fracture is considered ductile; mode B is cracking in the SnTe and substrate; mode C is cracking in the substrate. Each black circle spots correspond to the composition of the site by using EDS analysis. Figure 9 shows the percentage of the fracture mode in the systems. Figure 9a shows the fraction of the failure mode in the *n*-type Bi_2Te_3 system. We observed that the failure mode was mostly mode B and C when no diffusion barrier was used. The ball shear strength of SAC305/*n*-type Bi_2Te_3 is lower than Sn/*n*-type Bi_2Te_3. The results suggested that the thickness of SnTe in the SAC305/*n*-type Bi_2Te_3 system is higher than Sn/*n*-type Bi_2Te_3, and it increases the probability of cracking. After depositing Ni-P layers, the fracture modes are mostly mode A and mode B. Some fractures only occurred in the solder, while some fractures occurred both in the solder and in the substrate. According to EPMA, the composition at the fracture surface comprised Ni_3Te_2, Ni-P and *n*-type Bi_2Te_3 in mode B. The probability of mode A (ductile fracture) in Sn/Ni-P/*n*-type Bi_2Te_3 is higher than SAC305/Ni-P/*n*-type Bi_2Te_3. It leads to higher shear strength in Sn/Ni-P/*n*-type Bi_2Te_3. In the *p*-type Bi_2Te_3 system, Fig. 8b shows the top view of

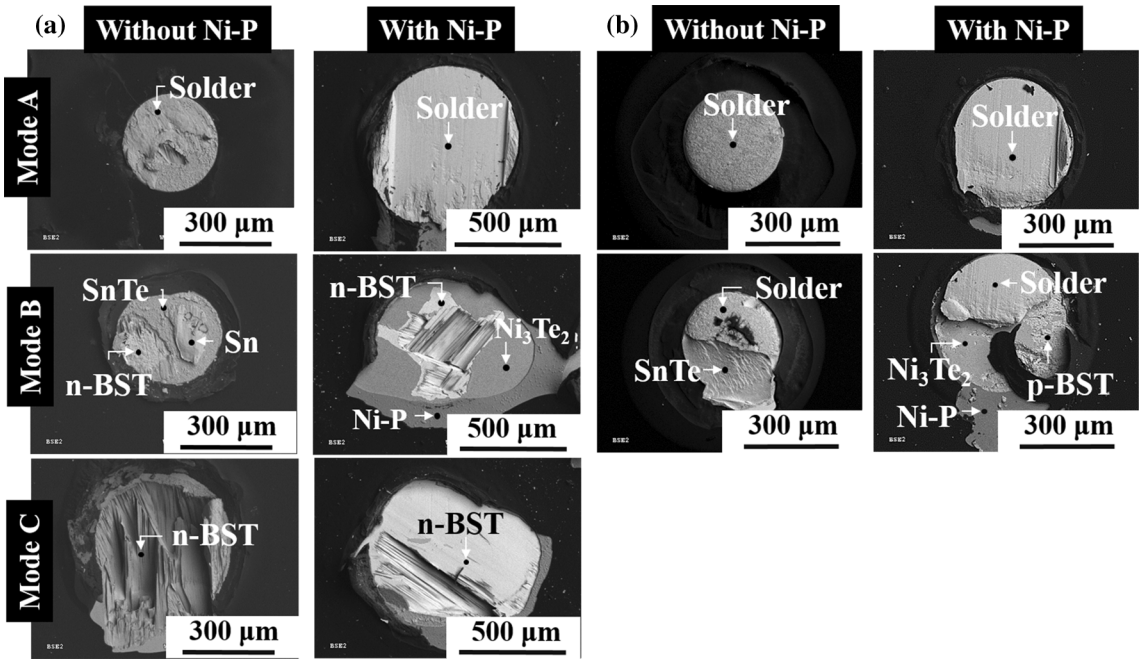

Fig. 8. The top views of the fracture surfaces for (a) *n*-type Bi_2Te_3 system (b) *p*-type Bi_2Te_3 system.

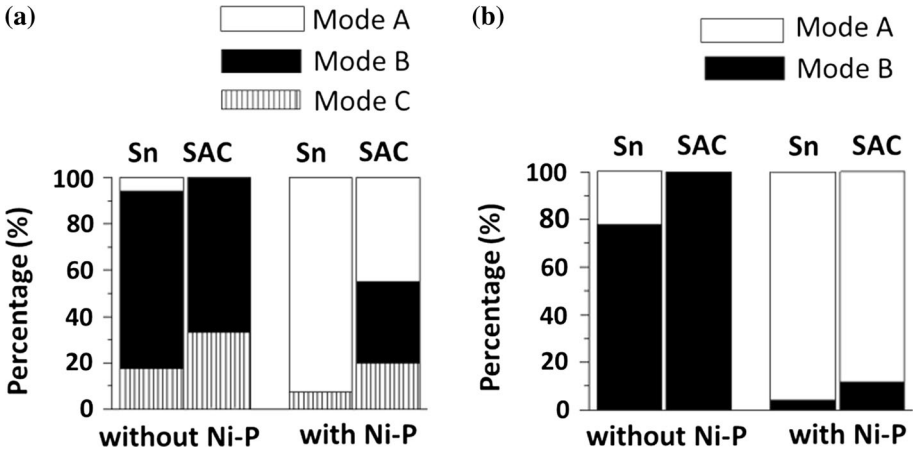

Fig. 9. The fraction of the failure mode in (a) *n*-type Bi_2Te_3 and (b) *p*-type Bi_2Te_3 sample.

the fracture surfaces of the solder joints after shear tests. Figure 9b shows that the failure mode mostly occurred in the SnTe. After depositing the Ni-P layer, the fracture mostly occurred in the solder instead of being at the SnTe interface and increased the shear strength in both systems. The improvement of the mechanical properties with Ni-P can be attributed to the inhibition of the formation of SnTe IMCs. Therefore, the electroless Ni-P not only suppressed the formation of SnTe IMCs but also improved the mechanical strength.

CONCLUSION

This study shows the electroless Ni-P layer can be an effective diffusion barrier to prevent the formation of porous SnTe layer when using Sn and SAC305 solder reacting with *n*-type Bi_2Te_3. When the Ni layer was deposited on *n*-type Bi_2Te_3, the dominant diffusion Te reacted with Ni and formed Ni_3Te_2 at the Ni-P side; Te reacted with the substrate to form a Bi-Te-Ni ternary alloy layer at the substrate side. The shear test was performed to compare the joint strength for Sn and SAC305 on *n*- and *p*-type Bi_2Te_3 with and without the diffusion barriers. With a Ni-P diffusion barrier, the joint strength are all higher than that without the layer. The fracture mode became more ductile when applying the barrier layer. It shows that the brittle and porous SnTe layer was successfully suppressed by the diffusion barrier.

ACKNOWLEDGEMENTS

The authors would like to thank the Ministry of Science and Technology for financially supporting this research under Contract No. 104-2221-E-008-065-MY3. We thank the Industrial Technology Research Institute of Taiwan for supplying samples. The help with EPMA analysis from Prof. Jeng Gong Duh and Ms. Tsai at National Tsing Hua University in Taiwan is greatly appreciated.

REFERENCES

1. L.E. Bell, *Science* 321, 1457 (2008).
2. G.J. Snyder and E.S. Toberer, *Nat. Mater.* 7, 105 (2008).
3. M.G. Kanatzidis, S.D. Mahanti, and T.P. Hogan, *Chemistry, Physics, and Materials Science of Thermoelectric Materials—Beyond Bismuth Telluride* (New York: Kluwer/Plenum, 2003), p. 1.
4. S.W. Chen and C.N. Chiu, *Scr. Mater.* 56, 97 (2007).
5. C.N. Chiu, C.H. Wang, and S.W. Chen, *J. Electron. Mater.* 37, 40 (2008).
6. Y.C. Lan, D.Z. Wang, G. Chen, and Z.F. Ren, *Appl. Phys.* 92, 101910 (2008).
7. O.D. Iyore, T.H. Lee, R.P. Gupta, J.B. White, H.N. Alshareef, M.J. Kim, and B.E. Gnade, *Surf. Interface Anal.* 41, 440 (2009).
8. W.S. Liu, H.Z. Wang, L.J. Wang, X.W. Wang, G. Joshi, G. Chen, and Z.F. Ren, *J. Mater. Chem. A* 1, 13093 (2013).
9. P.Y. Chien, C.H. Yeh, H.H. Hsu, and A.T. Wu, *J. Electron. Master.* 43, 284 (2014).
10. S.W. Chen, T.R. Yang, C.Y. Wu, H.W. Hsiao, H.S. Chu, J.D. Huang, and T.W. Liou, *J. Alloys Compd.* 686, 847 (2016).
11. T.Y. Lin, C.N. Liao, and A.T. Wu, *J. Electron. Mater.* 41, 153 (2012).
12. W.H. Chao, Y.R. Chen, S.C. Tseng, P.H. Yang, R.J. Wu, and J.Y. Hwang, *Thin Solid Films* 570, 172 (2014).
13. R.P. Gupta, K. Xiong, J.B. White, K. Cho, H.N. Alshareef, and B.E. Gnade, *J. Electrochem. Soc.* 157, H666 (2010).
14. C.Y. Ko and A.T. Wu, *J. Electron. Mater.* 41, 3320 (2012).
15. J. Jiang, L. Chen, Q. Yao, S. Bai, and Q. Wang, *Mater. Chem. Phys.* 92, 39 (2005).
16. J.W.G. Bos, H.W. Zandbergen, M.-H. Lee, N.P. Ong, and R.J. Cava, *Phys. Rev. B* 75, 195203 (2007).
17. L.C. Lo and A.T. Wu, *J. Electron. Mater.* 41, 3325 (2012).
18. C.N. Liao, C.H. Lee, and W.J. Chen, *Electrochem. Solid State Lett.* 10, 23 (2007).
19. S.W. Chen, C.Y. Wu, H.J. Wu, and W.T. Chiu, *J. Alloys Compd.* 611, 313 (2014).
20. Y.C. Lin, K.J. Wang, and J.G. Duh, *J. Electron. Mater.* 39, 283 (2010).